A quantitative analysis of electronic transport in n- and p-type modulation-doped GaAsBi/AlGaAs quantum well structures

Omer Donmez[1,*], Ayse Erol[1], Çaglar Çetinkaya[1], Erman Çokduygulular[2], Mustafa Aydın[1], Saffettin Yıldırım[1], Janne Puustinen[3], Joonas Hilska[3], Mircea Guina[3]

[1]Department of Physics, Faculty of Science, Istanbul University, Vezneciler, 34134, Istanbul, Turkey

[2]Department of Engineering Science, Faculty of Engineering, Istanbul University-Cerrahpasa, 34320 Avcılar, Istanbul, Turkey

[3]Optoelectronics Research Centre, Physics Unit, Tampere University, Korkeakoulunkatu 3, 33720 Tampere, Finland

*E-mail: omerdonmez@istanbul.edu.tr

Abstract

Electronic transport properties of as-grown and thermally annealed n- and p-type modulation-doped GaAsBi/AlGaAs quantum well (QW) structures were investigated. Hall mobility of as-grown, n- and p-type modulation doped QW structures are found from raw experimental data as ~ 1414 and 95 cm^2/Vs at room temperature. A comparison between reported two dimensional (2D) electron density determined from the analyses of Shubnikov de Haas (SdH) oscillations and the 2D Hall electron density indicates a presence of parallel conduction in barrier layer (AlGaAs) and QW layer (GaAsBi) in n-type samples, therefore a parallel channel conduction theory is used to separate the electron mobility in the QW and the barrier layers in n-type modulation doped GaAsBi/AlGaAs QW structure. The extracted electron mobility of the as-grown n-type GaAsBi/AlGaAs QW sample is determined as ~ 5975 cm^2/Vs at 4.2 K, which is closer to the electron mobility in GaAs. It is found that thermal annealing at lower temperature than growth temperature increases electron mobility of 2D electron gas, while annealing at higher temperature than growth temperature decreases electron mobility. The temperature dependence of the extracted electron mobility using parallel conduction approximation is analytically calculated by considering possible scattering mechanisms. Analysis of temperature-dependent electron mobility shows that the dominant scattering mechanisms are interface roughness, acoustic, and alloy-potential scatterings at low and intermediate temperature range, and interface roughness and optical phonon scattering at the high-temperature range in n-type modulation doped GaAsBi/AlGaAs QW structures.

Keywords: modulation doped GaAsBi, electron mobility in GaAsBi, hole mobility in GaAsBi, parallel conduction

Introduction

Since the discovery of the dramatic influence of Bi alloying on the valence band structure of GaAs, bismide alloys have become attractive due to Bi-related band tailoring effects as well as promising properties for optoelectronic devices [1–3]. Electron and hole transport properties and mechanisms in these optoelectronic devices have vital importance for controlling and manipulating the functionality of the devices. The transport mechanism of the electron and hole depends on the electronic band structure of the devices as well as design and dimension of the devices. An electronic band structure of the Bi containing III-V alloys is expressed with Valence Band Anti-Crossing Model (VBAC) with virtual crystal approximation (VCA). The VBAC model with VCA projection for valence bands (VB) are strongly re-constructed with the incorporation of the Bi atom, while conduction (CB) is slightly altered so it is expected that the electron transport properties slightly deteriorated. Fluegel *et al.* reported that electron mobility in GaAsBi layers tends to decrease with Bi up to 0.88% Bi, due to the weak effect of the Bi on the CB[4]. Kini *et al.* reported that the electron mobility in intentionally doped GaAsBi epilayer on SI-GaAs is not significantly affected by introducing Bi atoms into GaAs for up to 1.2% Bi content, while it substantially deteriorates with Bi content higher than 1.6% for n-type GaAsBi epilayers [5]. Cooke *et al.* also investigated electron mobility in unintentionally doped GaAsBi epilayer on GaAs and AlGaAs layer utilizing time-resolved terahertz spectroscopy measurements [6,7]. They found that electron mobility is independent of the substrate/buffer layer for ~0.9%Bi, the samples grown on GaAs and AlGaAs are almost independent of the presence of the Bi atom in GaAs for up to 1.4% but degrades after 1.4%Bi. Kini *et al.* revealed that hole mobility in Be-doped GaAsBi epilayer is deteriorated by incorporation of the Bi [8]. Pettinari *et al.* reported that resistivity of the GaAsBi epilayer is very high, so hole mobility of the nominally undoped GaAsBi could be measured at a high magnetic field, higher than 10 T [9]. Contrary to these reported hole mobility results, Kado *et al.* disseminated that hole mobility in the Be-doped GaAsBi with ~4%Bi is comparable to p-type GaAs grown at nominal temperature, but above 5% Bi, the hole mobility degrades [10]. So far, all reported studies have been carried out on bulk or epilayer forms of p-type GaAsBi structures.

The efficiency and performance of the optoelectronic devices improve by decreasing the dimensionality of the design. When dimensions of the GaAsBi is reduced, it is seen weak conduction band offset or confinement of the electron in CB for low Bi content, due to the weak interaction of the Bi with CB. In order to overcome the weakness, one way is to exploit large bandgap material for barrier layers. Ludewig *et al.* showed that this AlGaAs layer for the barrier is good at carrier confinement within QW layers[11]. Contrary to bulk and epilayer GaAsBi materials, there are limited studies on the investigation of the electrical transport mechanism of the low dimensional GaAsBi structures apart from our previously published papers [12,13]. In our previous studies on n-type modulation doped GaAsBi/AlGaAs QW structures, we determined fundamental electrical transport parameters such as electron effective mass, quantum mobility, the carrier density in QW, Fermi level position, and deformation potential energy at low temperatures [12,13]. So far, there have not been any reports about the analyses of temperature dependent electron mobility in Bi-containing QW structures, which is important to have a knowledge on temperature dependent characteristic of carrier mobility at the stage of designing electronic and optoelectronic devices based on Bi-containing QW structures.

In this paper, we investigate the temperature dependent characteristics of electron and hole transport mechanisms in as-grown and post-growth thermally annealed modulation-doped n- and p-type $Al_{0.15}Ga_{0.85}As/GaAs_{0.96}Bi_{0.04}$ QW structures. A parallel conduction theory is used to extract true temperature dependence of 2D electron gas in GaAsBi/AlGaAs QW. We have analytically calculated the possible scattering mechanisms, and dominant scattering mechanisms limiting the electron mobility are determined at different temperature ranges. In the analytical calculations of possible scattering-limited electron mobility, we have utilized the fundamental transport parameters reported in our previous study [12,13]. We have also presented the temperature dependence of Hall mobility and 2D hole density for p-type modulation doped GaAsBi/AlGaAs QW structures down to 160 K. At temperatures lower than 160 K, the resistivity of the as-grown and annealed p-type samples have drastically increased, which we attribute to the trapping of free holes.

Experimental Methods

In order to determine the effects of Bi and thermal annealing on the electronic transport properties of the 2D electron and hole gases, n-and p-type modulation-doped $GaAs_{1-x}Bi_x/Al_{0.15}Ga_{0.85}As$ QW samples were grown on SI-GaAs substrates by molecular beam epitaxy (MBE). The sample structures are given in Table

I. The GaAsBi layer in the samples was grown at 370 °C, and the other layers were grown at 580 °C. The Bi composition of alloy compositions was determined by HR-XRD measurement as 4%. The growth details can be found in Refs. [12,13]. The Bi-free reference GaAs/AlGaAs QW sample has an identical structure but the QW layer does not contain Bi atoms, and is grown at the typical growth temperature.

Table I: Schematic diagram of the grown samples used in this study. Si and Be are used for n-and p-type doping, respectively.

Material	**Thickness (nm)**	**Dopant type /density**
GaAs (cap)	5	Si/Be- $5 \times 10^{17}\text{cm}^{-3}$
$Al_{0.15}Ga_{0.85}As$ **(**barrier)	10	Si/Be -1$\times 10^{18}\text{cm}^{-3}$
$Al_{0.15}Ga_{0.85}As$ (spacer)	5	Undoped
$GaAs_{0.96}Bi_{0.04}$ (quantum well)	7	Undoped
$Al_{0.15}Ga_{0.85}As$ (spacer)	5	Undoped
$Al_{0.15}Ga_{0.85}As$ (barrier)	10	Si/Be-1 $\times 10^{18}\text{cm}^{-3}$
GaAs buffer layer		
GaAs semi-insulating substrate		

Post growth rapid thermal annealing was applied under N_2 gas flow at 700 °C (higher than the growth temperature of the GaAsBi layer) for the 60 s for n- and p-type samples, and 350 °C (lower than growth temperature) for 180 s for n-type samples. Since we did not obtain clear signal for all p-type samples at temperatures lower than 160 K, we will only present experimental results between 160 and 300 K. However, we report a detailed analysis of effect of the annealing on the temperature dependent electronic transport properties of the 2D electron gas at temperature range between 4.2 and 300K. We have analyzed the electronic transport of two n-type samples, annealed at 350 °C and annealed 700 °C. Afterall, we give the results for all as-grown and annealed n- and p-type samples, but we have only analyzed the electronic transport properties of as-grown and annealed n-type samples at 350 °C and 700 °C.

The electronic transport properties of the two dimensional (2D) electron were studied using the orthodox Hall Effect method [14]. In this method, a fixed magnetic field is employed perpendicular to current density, but parallel to the growth direction. Bruker Hall Effect System with a 2T copper coil electromagnet at 4 cm distance between coils and Oxford-Heliox-VL ^{3}He cryostat equipped with an 18T superconducting magnet were used to carry out Hall Effect measurements between 77 K-300 K and

between 2 K-80 K, respectively. All samples were defined with standard photolithography techniques as having a Hall bar geometry with a length of 1.75 mm and a width of 0.7 mm. Au(200 nm)/Ni(20 nm)/Au:Ge(120 nm)/Au(5 nm) and Au(200 nm)/Ti(20 nm) contacts were fabricated using thermal evaporation technique using a VAKSIS Twin Chamber Thermal Evaporator system for n- and p-type samples, respectively. A fixed 50 μA current was applied to the samples during the measurements.

Analytic Modeling of Temperature Dependence of Electron Mobility

Here, we present analytical modeling of the temperature dependence of electron mobility considering all possible scattering mechanisms, which restrict carrier mobility and are well-defined in the literature. The temperature dependence of hole mobility could be determined at a limited range of temperatures due to the extremely high resistance of the p-type samples at temperatures lower than 160 K; therefore, we have only modeled the temperature dependence of the electron mobility. In the calculations, electron effective mass, 2D electron densities, and Fermi levels in n-type samples are essential parameters and obtained from the analyses of the SdH oscillations in our earlier paper[12]. It is known that the analyses of the SdH oscillations give the 2D electron density, when SdH oscillations is observed in 2D systems. On the other hand, Hall effect measurements give not only the 2D electron density in the QW layer but also the total electron density in heterostructures in the case of any parallel conducting layers from out of the QW layer. Especially, in modulation-doped heterostructures, parallel conduction from the doped barrier layer is a common observation [15,16]. A comparison between electron densities obtained from Hall Effect measurements and analyses from SdH oscillations presented in one of our recent papers (see Table II for the values of electron densities) indicates that the electrons in the barrier layer (AlGaAs) also contribute to the electronic transport for all n-type samples studied here[12]. We have discussed the analyses of the SdH results in our recent papers [12,13]; therefore, we will only use the determined material parameters (effective electron mass, Fermi level, and 2D electron density) from SdH oscillations in the calculations. We have shown for n-type samples that the 2D electron gas occupies the states in both GaAsBi QW and AlGaAs barrier layer for all n-type samples. Therefore, we will also consider scattering mechanisms for electrons in the barrier AlGaAs layer.

It is worth noting that components of the conductivity tensor can be separated with a simple parallel conduction extraction method (SPCEM), multi-carrier fitting procedure (MCF), mobility spectrum analysis (MSA), improved quantitative mobility spectrum analysis (i-QMSA), *etc*. [15,17–19]. In order

to separate the contribution of each layer to total conductivity, the well-known Hall Effect should be measured under low different magnetic field values and some strict assumptions are required. Also, in our previous studies, parallel conduction is analyzed with the SPCEM model with strict assumptions [16]. However, we separate parallel conduction mechanisms using a low magnetic field measurement (Hall effect) and previously reported magnetoresistance results without making any assumptions in this study. Then, the extracted temperature dependence of electron mobility of 2D electron gas in GaAsBi/AlGaAs QW structures is quantitatively analyzed using all possible scattering mechanisms, which limits electron mobility.

In order to evaluate the temperature dependence of the electron mobility in the QW and barrier layer, different scattering mechanisms affecting the temperature dependence of the electron mobility have been considered as given below, and the total mobility is calculated with the well-known Matthiessen's rule, expressed as[17]

$$\frac{1}{\mu_{total}} = \sum_i \frac{1}{\mu_i} \tag{1}$$

where μ_i is attributed to different scattering mechanisms.

The possible scattering mechanisms limiting electron mobility in n-type samples are briefly defined below.

i) *Ionized impurity scattering* limited electron mobility (μ_{II})

Since the barrier layer ($Al_{0.15}Ga_{0.85}As$) is doped and some of the electrons occupy the states in the barrier layer, we consider the ionized impurity scattering mechanism, one of the dominant scattering centers at low temperatures. In this layer, both electrons and their parent donor ions are in the same space; hence ionized impurity scattering mechanism must be included. The standard definition of the ionized impurity scattering limited electron mobility is formulated as

$$\mu_0 = \frac{64\sqrt{\pi(2k_BT)^3}\,\varepsilon^2}{NZ^2e^3\sqrt{m_e}} f(T)^{-1} \tag{3}$$

where N is a number of the ionized impurity center, Z is a charge on ionized impurity, m_e is the electron effective mass, ε is the dielectric constant of AlGaAs and k_B is the Boltzmann constant. $f(T)$ is a temperature-dependent parameter; it must be solved under boundary conditions to obtain analytical

results. It is well-known that ionized impurity scattering has a temperature dependence of $T^{3/2}$. Eq. 3 is then modified as a function of electron density for un-screened (Conwell-Weisskopf (C-W) model)[20], screened (Brooks-Herring (B-H) model)[21–23], the intermediate case between screened and un-screened[24], and strongly degenerate case[25]. We have found that the 3D electron density in the barrier layer, by subtracting Hall carrier density from the carrier density determined from SdH oscillations to determine which regime is applicable for our samples. Using the obtained 3D electron density values in the un-screened, screened, intermediate, and strong degeneration formulas for ionized impurity scattering limited electron mobility, we have calculated the temperature dependence of electron mobility as shown in Figure 1. It is obvious that the models for unscreened, intermediate and screened regimes do not exhibit a well-known $T^{3/2}$ characteristic of the ionized impurity scattering. Szmyd *et al.* defined a limit for the strong degeneration for $n_{3D} \geq 4 \times 10^{18} cm^{-3}$for n-type GaAs [25]. For the as-grown n-type Bi-free sample (reference sample), at ~4K, $n_{3D} = 4.6 \times 10^{18} cm^{-3}$, satisfying the strong degeneration condition. For strong degeneration, ionized impurity scattering limited electron mobility is expressed by Szmyd *et al.* as

$$\mu_{II} = 3\varepsilon_0^2 \left(\frac{h}{e}\right)^3 \left(\frac{n_{3d}}{N_{dop}}\right) \left(\frac{1}{m_e}\right)^2 (\ln(1+\xi) - \xi/(1+\xi)\ )^{-1} \quad (4)$$

where ξ is defined as $16\varepsilon_0 m_e E_F / 3e^2 n_{3D} \hbar^2$. In our cases, the 3D carrier density is higher than $4 \times 10^{18} cm^{-3}$. The result of Eq. 4 is almost independent of the temperature because the scattering of the electrons by ionized impurities is screened, as shown in Figure 1.

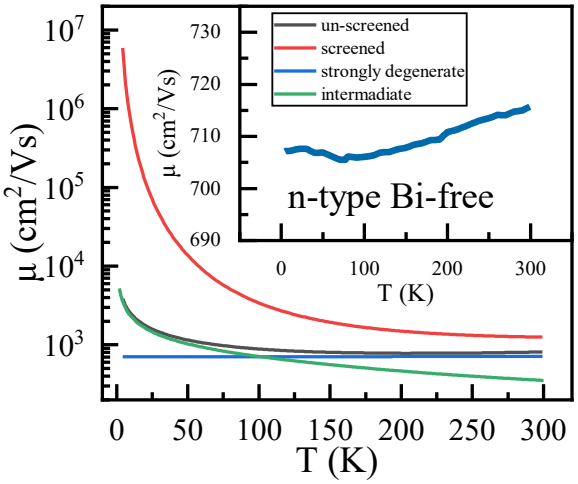

Figure 1. Calculated temperature dependence of the electron mobility limited by ionized impurity scattering for the barrier layer (AlGaAs) in the n-type Bi-free sample. Inset shows the enlarged results for the strongly degenerate case, used in analytical mobility calculation for n-type samples.

ii) *Remote ionized impurity scattering limited electron mobility (μ_{RII})*

In modulation-doped heterostructures, electrons and their parent donor ions are separated from each other with a spacer layer, and electrons in the QW layer are affected with positively charged ions in the barrier layer via remote Coulomb interactions, and the electron mobility is defined under the influence of remote ionized scattering as [16,26]

$$\mu_{RII} = \frac{\left(64\pi\hbar^3\varepsilon_0 S_0^2 (2\pi n_{2D})^{3/2}\right)^2}{e^3 m_e}\left[\frac{1}{L^2} - \frac{1}{(d+L)^2}\right]^{-1} \quad (5)$$

where n_{2D} is the 2D electron density in QW, d is the thickness of the spacer layer, L is the width of the QW, and S_0 is the screening constant for the degenerate case.

iii) Acoustic phonon scattering limited electron mobility μ_{AP}

Acoustic phonon scattering is defined with deformation potential and piezoelectric phonon scatterings. The expression for the deformation potential is given by [27,28]

$$\mu_{def} = \frac{16\rho e v_L^2 \hbar^3}{3\Xi^2 k_B T\, m_e^2\, b_{ap}\, J_{dp}(k)} \quad (6)$$

where ρ is the density of the crystal, v_L is the velocity of longitudinal acoustic phonons, Ξ is deformation potential, b_{ap} is Fang-Howard expression, and the J_{dp} is a function of inverse screening length. Piezoelectric acoustic phonon scattering-limited mobility is expressed by [27,28]

$$\mu_{pie} = \frac{\pi\hbar^3\varepsilon_0 k}{eK_{av}^2 k_B T m_e^2 J_{pie}} \quad (7)$$

where K_{av} is the electromechanical coupling constant and J_{pie} is a function of inverse screening length.

The overall acoustic phonon scattering is defined as $1/\mu_{AP} = 1/\mu_{pie} + 1/\mu_{def}$.

iv) Optic phonon scattering (OP)

Ridley derived the equation for the polar optical phonon scattering-limited mobility as [27]

$$\mu_{po} = \frac{4\pi\hbar^2\varepsilon_0\varepsilon_p}{e\omega_{po}m_e^2L_F}\left[\exp\left(\frac{\hbar\omega_{po}}{k_BT}\right) - 1\right] \quad (8)$$

where ε_p is related to dielectric constant, $\hbar\omega_{po}$ is the polar optic phonon energy, $\varepsilon_s$ve ε_∞ are the high and low-frequency dielectric constants, m_e is the carrier effective mass, and L_F is the effective thickness of the layer. This model is used for the barrier layer and QW. Therefore, the L_F is calculated from inverse 3D and 2D Fermi wave vector for barrier layer and QW, respectively.

v) Alloy scattering (μ_{ALL})

Alloy disorder scattering- limited mobility is calculated by the following expression[29]:

$$\mu_{ALL} = \frac{16e\hbar^3}{3b_{ALL}x(1-x)\Omega_0U_{all}^2} \quad (9)$$

where Ω_0 is the volume of primitive cell, x is the alloy content, and U_{all} is the alloy potential for ternary alloys, and b_{ALL} is the self-consistent Hartree expression. In the alloy potential calculation, the strain effect is included.

vi) Interface Roughness scattering (μ_{IFR})

Interface roughness scattering (IFR) for screened/degenerate cases is given as

$$\mu_{IFR} = \frac{\pi\hbar^3}{e^3J_{IFR}} \quad (10)$$

where the J_{IFR} is the function of the inverse screening length, the lateral size Λ and height Δ of the Gaussian fluactuation, 2D carrier density in QW. J_{IFR} is analytically solved for degenerate cases [30].

All parameters used in the calculations are given in Table II, together with experimentally obtained parameters.

Table II: The material parameters at ~ 4.2 K used in scattering calculations. GaAs-related parameters are taken from Ref.[31] and GaAsBi-related parameters are taken from Refs [32–35]. Some parameters are determined from the present study and ascribed as (exp.) in Table. The second subband parameters for Bi-free sample (TNR00) and Bi-containing sample annealed at 350 °C (TNBi04B) are given in bracket.

Parameters	Symbol	TNR00	TNBi04	TNBi04A	TNBi04B
Electron effective mass, *(Exp.)*[12]	m_e^* (m_e)	0.080 (0.073)	0.077	0.078	0.076 (0.066)
Fermi Level, *(Exp.)*[12]	$(E_F - E_i)$ (meV)	121 (58)	80	111	127 (63)
2D electron density	n_{2D} (10^{16}m^{-2})	3.96 (1.76)	2.56	3.6	4.03 (1.73)
Hall Effect carrier density	n_{Hall} (10^{16}m^{-2})	11.64	11.61	9.09	10.7
Deformation potential, (*Exp*.) [13]	Ξ (eV)	9.5 (7)	7.3	0.5	4 (4.2)
Crystal density[31,34]	ρ (10^3kg/m^3)	5.32	5.44		
Sound velocity[31,34]	v_L (10^3m/s)	4.79	4.75		
Electromechanical coupling constant[31,34]	K_{av}^2	0.025	0.045		
Dielectric constant[33,35]	ε (ε_0)	12.9	11.3		
Elastic constants[31,34]	C_{11} (10^{11}dyn/cm^2)	12.21	7.3		
Elastic constants[31,34]	C_{12} (10^{11}dyn/cm^2)	5.66	3.27		
Elastic constants[31,34]	C_{44} (10^{11}dyn/cm^2)	6	3.6		
Piezoelectric stress constant[36]	e_{14} (C/m^2)	-0.16	-0.16		

Results and Discussion

a) Experimental results

Figure 2 (a) and (b) shows the temperature dependence of carrier mobility and 2D carrier density for as-grown and annealed Bi-free and Bi-containing GaAsBi/AlGaAs QW samples. The p-type as-grown sample's resistivity is too high (over 500 MΩ at 230 K) to measure the Hall effect between ~2 K and 240

K. Hence, we could obtain consistent/stable mobility only above 240 K. The Bi atom is likely to generate a deep potential trap for the holes, which has activation energy at around room temperature and releases trapped holes around 240 K. Therefore, we suggest that holes are captured by the deep level defect and are emitted at approximately 240 K.

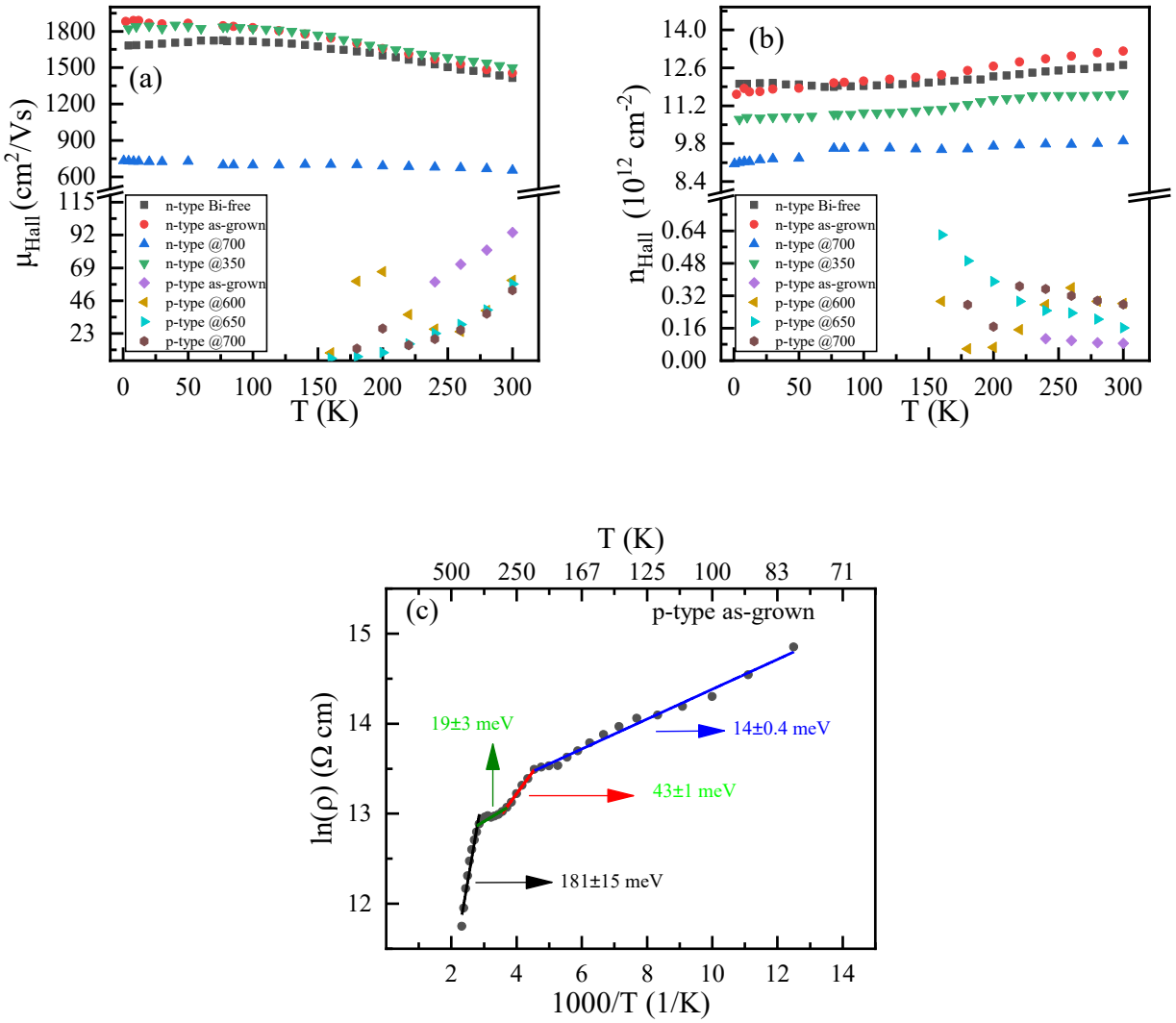

Figure 2. Temperature dependence of the Hall effect results: **(a)** carrier mobility, and **(b)** carrier concentration in as-grown and annealed samples. **(c)** Temperature-dependent resistivity of the p-type as-grown samples.

To confirm this, the temperature dependence of the resistivity is determined, and several activation energies are determined from slop of Arrhenius plot, as seen in Figure 2 (c). We have found three activation energies as well as a deep level defect at activation energy of 180 meV, which could be

responsible for hole depletion below 240 K in p-type samples. It is worth noting that our Hall effect systems are limited to a temperature below 300 K. Therefore, we could not carry out the Hall effect measurement above 300 K. Even the defect states is strongly dependent on the growth conditions [37–42], the determined defect energy levels in this study are closed to the literature [43]. The hole mobility varies in the range of 60-95 cm^2/Vs between 240 K and 300 K for the as-grown sample, which is smaller than the hole mobility in the Bi-free p-type sample, which fulfils the VBAC model. Pettinari *et al.* found that the hole mobility is 10 cm^2/Vs for a p-type GaAsBi epilayer with Bi composition of 3.8%[9]. The higher hole mobility observed in p-type modulation-doped samples is a result of the decreasing interaction between ionized acceptors in the barrier layer and holes in the QW. As seen in Figure 2(a), annealing does not enhance the hole mobility due to the increment in hole density upon annealing. Increased hole density upon thermal annealing can result from the release of the captured holes by impurities having low activation energies. It is also obvious that the electron mobility in the as-grown Bi-containing sample (TNBi04) is higher than that of electron mobility in Bi-free n-type sample (TNR00), which can be related to the surfactant effect of Bi [44,45]. Even as the n- and p-type samples are doped at the same nominal density of the dopant atoms, the electron density is about two orders of magnitude of holes, which can also be a suggestion of high-density acceptor-like defects in both p-type Bi-free and Bi-containing samples due to low temperature growth conditions. The electron mobility becomes smaller upon annealing above the growth temperature of GaAsBi (700 °C, TNBi04A) but is negligibly affected from annealing at 350 °C. It is worth noting that the electron mobility values obtained from both Hall effect and SdH analyses are so small even for the Bi-free sample for typical modulation-doped structures. So far, we have presented the experimental parameters obtained from SdH analyses without a discussion on the electron Hall mobility values and only compared the results with those of a Bi-free sample in our previously published papers [12,13]. It is evident from a comparison of Hall effect results and SdH analyses that electrons occupy the states in both the QW and the barrier layers; hence the overall mobility is affected from both channels. To analyze the temperature dependence of the electron mobility, first, the contributions to the electron mobility from the QW and the barrier layers have to be distinguished. After the separation, the effects of Bi alloying and annealing process can be interpreted appropriately. To do that, the temperature dependence of 2D and 3D electron densities has to be determined.

The electron density in the QW layer up to 40 K was determined from Shubnikov-de Hass (SdH) oscillations for all n-type samples and depicted in Figure 3. We found that the electrons occupy the first

subband in the Bi-containing as-grown (TNBi04) and thermally annealed at 700 °C(TNBi04A) samples, whereas they occupy the first two subbands in the Bi-free (TNR00) and annealed Bi-containing at 350 °C (TNBi04B) samples [12]. It is evident that the 2D carrier density is almost independent of the temperature between 2 K - 40 K. It is known that SdH oscillations give only the electron density in the QW for our sample structures under certain experimental condition (given in the Experimental method section), whereas the Hall effect gives the total electron density in the entire sample structure [46]. As clearly seen in Figures 2(b) and 3(a), the 2D carrier density determined from SdH oscillations is lower than that derived from the Hall Effect, indicating that the electrons occupy both the QW and barrier layer. Therefore, it is evident that there is parallel conduction in n-type modulation-doped samples.

As we have shown in the band-profile calculations in our recent paper on these samples [47], electrons are well-confined in the GaAsBi QW layer thanks to the sufficiently high bandgap discontinuity between $Al_{0.15}Ga_{0.85}As$ and GaAsBi QW, preventing escaping of electrons from the QW. Therefore, to determine the temperature-dependent electron density in QW in the temperature range of interest, we can exploit the 2D electron density formula given as

$$n_{2D}^{i} = \left(\frac{m_e^i}{\pi\hbar^2}\, k_B T\right) \ln\left(1 + \exp\left(-\frac{E_i - E_F}{k_B T}\right)\right) \tag{11}$$

where, m_e and $E_F - E_i$ are determined from SdH measurements. $\hbar$ and k_B are fundamental physical constants. As seen in Figure 3(a), the calculated temperature-dependent carrier density matches with experimental values recorded up to 40 K, which allow us to extrapolate the 2D electron density in the QW layer to the whole temperature range of interest. According to Eq. 11, the temperature-dependent 2D carrier density has a weak temperature dependence, which can also be seen in Figure 3(a). After the determination of the temperature-dependent electron density in the QW with Eq. 11, we can obtain the electron density in the barrier layer by subtracting the obtained values of the 2D carrier density as a function of temperature from the values of electron density determined from the Hall Effect measurements (Figure 2(b)).

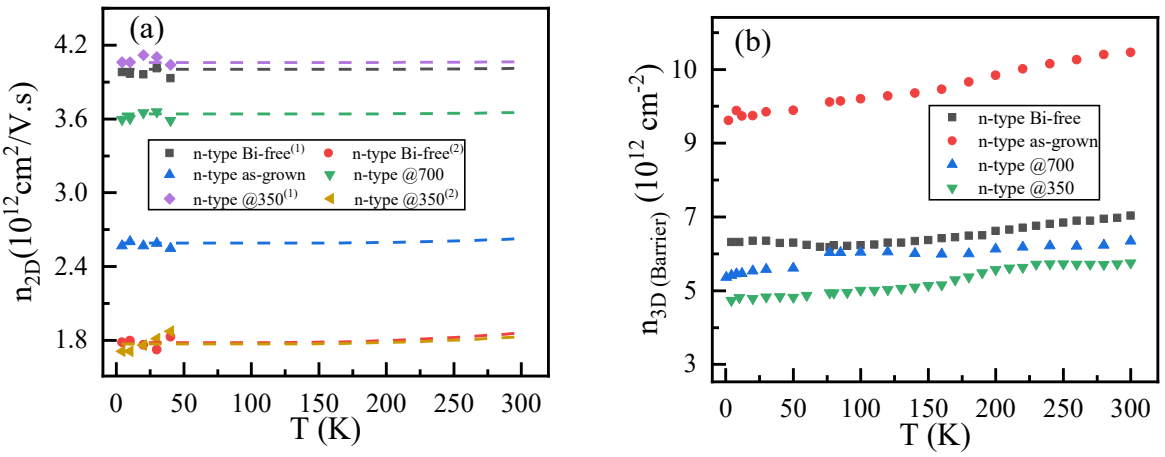

Figure 3. Temperature-dependent a) 2D electron concentration in the QW and b) extracted carrier density in the barrier layer. The first and second subband results for the Bi-free (TNR00) and Bi-containing samples annealed at 350°C (TNBi04B) are labeled in the bracket.

Considering Figures 2(b), 3(a), and 3(b), it is clear that most of the electrons are in the barrier layer, which indicates that states in the QW are not sufficient to be occupied by electrons. The highest electron density is observed in the barrier layer of the as-grown Bi-containing sample (TNBi04). There are two occupied subbands in the as-grown Bi-free sample (TNR00) and the Bi-containing sample annealed at 350 °C (TNBi04B). With Bi incorporation, the bandgap redshifts, and the effective electron mass decreases; therefore, the e1 subband is occupied in the as-grown Bi-containing sample (TNBi04), resulting in a higher electron density of electrons in the barrier layer. Upon annealing, several factors can affect the change of the electron densities in the barrier layer, such as bandgap, barrier height, effective mass, the number of the available subbands in QW, and effects of annealing on electron density are explained in details in our previous paper[12]. We can conclude that the number of the available subbands to be occupied and effective electron mass in GaAsBi QW, which is responsible for the density of states of the subbands in the QW, changes the electron density of the barrier layer.

b) Quantitatively analyzing the temperature dependence of electron mobility

It is shown that the electrons occupy both the QW and barrier layer, which is an indication of the parallel conduction in $Al_{0.15}Ga_{0.85}As/GaAs_{1-x}Bi_x$ (x=0.0, and 0.04). In the case of parallel conduction, the conductivity can be expressed as[15]

$$\sigma_{xx} = \sum_i \frac{en_i\mu_i}{1+(\mu_i B_z)^2} \quad (12)$$

where μ_i and n_i are the mobility and electron density of the ith channel, respectively. The conductivity of the samples has been determined from longitudinal and transverse magnetotransport measurements. We experimentally determined carrier densities in the barrier and QW layers, so we need to know electron mobility in the barrier layer or QW layer to extract the mobility in one of the parallel channels using Eq. 12. The barrier layer of the n-type modulation-doped samples is AlGaAs, and fortunately, the optical and electrical properties of the $Al_xGa_{1-x}As$ ($0 \leq x \leq 0.45$) alloy are well-known [36]. Hence, we can calculate the electron mobility in $Al_{0.15}Ga_{0.85}As$ (bulk/epilayer). Considering the determined 3D carrier density given in Figure 3(b) for the barrier layer, we have calculated temperature-dependent electron mobility in $Al_{0.15}Ga_{0.85}As$ considering the dominant scattering mechanisms including ionized impurity, acoustic and optic phonon scatterings, as given in the analytical modeling section. All parameters used in the calculations are listed in Table II. The calculated temperature-dependent electron mobility in the AlGaAs barrier layer are presented in Figure 4 for all n-type samples, and their values are in good agreement with the literature [48]. The highest electron mobility in the barrier layer belongs to the Bi-containing as-grown sample (TNBi04, see Table II and Figure 4). The change of the electron mobility as an effect of annealing in the barrier layer results from changed electron density upon annealing.

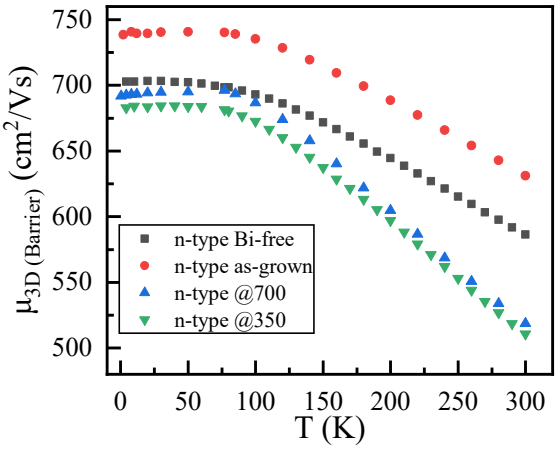

Figure 4. Temperature dependence of the calculated electron mobility of the barrier (bulk/epilayer) layer ($Al_{0.15}Ga_{0.85}As$, taking into account the Ionized impurity and optical phonon scatterings.

The electron mobility of the as-grown GaAsBi (TNBi04) QW layer is extracted using Eq. 12 with the condition $\omega_i \tau_i \ll 1$, the electron mobility in the barrier layer and the temperature-dependent characteristic analyzed using possible scattering mechanisms. As an example, Figure 5 shows that the temperature dependence of electron mobility in the as-grown Bi-containing sample (TNBi04) together with all possible scattering mechanisms. Figure 5 shows that calculated electron mobility matches with the extracted 2D electron mobility. To clarify the temperature-dependent scattering mechanisms that limits electron mobility, we separate the temperature regimes into two sub-regions: i) $2 < T \leq 150$, and ii) $150 \leq T < 300$. The dominant scattering centre are the alloy potential scattering, acoustic phonon for $2 < T \leq 150$ and are the optic phonon for $150 \leq T < 300$. We split into two temperature regions, interface roughness scattering is almost dominant in both i and ii) regions. In the analytical calculations, the lateral size Λ is calculated from the mean value of Fermi wavelength ($\sqrt{2\pi n_{2D}}$) and the height of roughness (Δ) is chosen as fitting parameters. The analytically calculated electron mobility with parameters given in Table II does not fit perfectly to the experimental value in the high-temperature region (see Figure 6, dotted-line), due to the weak interaction of the electron-optic phonons. Similar behavior was observed for counterpart of Bi-containing QW structure, N-containing dilute nitride QW structures and attributed to screening of the electron-optic phonon interaction [16,49]. Hence, the origin of the mismatching at high temperature region may be a screening of the electron-optic phonon interaction in GaAsBi QW. In order to obtain a good match to experimental results, we added a coefficient for the Fermi-wave vector in analytical calculations. The effective scattering mechanisms are alloy disorder potential, acoustic phonon, interface roughness scattering, and optical phonon scattering for all samples. The remote ionized impurity scattering does not affect the electron mobility for all the samples.

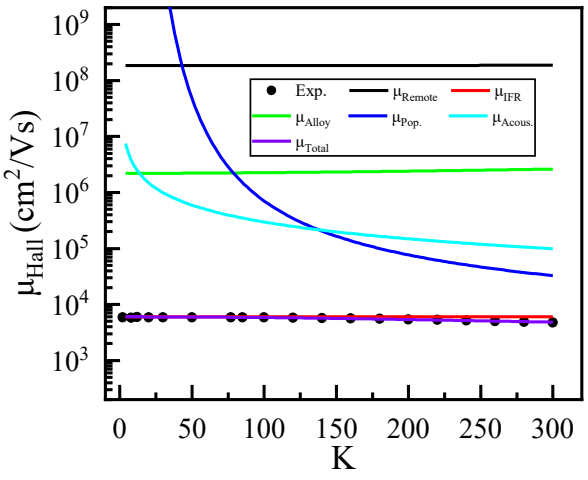

Figure 5. Experimental results with calculated possible scattering mechanism for as-grown TNBi04. Symbols and solid lines are ascribed for experimental and calculated results, respectively.

Figure 6 shows the extracted and analytically fitted temperature dependence of 2D electron mobility for all the samples. Since the Bi-free and annealed Bi-containing sample (TNBi04B) have two subbands occupied, we have also presented the electron mobility in the second subband for these samples. To determine the parallel transport among the barrier layer, the first and second quantized levels for the Bi-free (TNR00) and Bi-containing annealed at 350 °C (TNBi04B), we use electron density in each subband given in Table II. Typically, it is expected that the electron mobility in each subband is directly proportional to the carrier density in the QW [50,51]. However, Zheng *et al*. reported that the electron mobility in each layer is inversely proportional to carrier density due to interface induced effects [52]. In reported studies[12], the proportion between carrier density and electron mobility is seen from Hall mobility. Our results show that the first subbands are more populated with a factor of two in Bi-free (TNR00) and Bi-containing samples annealed at 350 °C (TNBi04B, see Table II), and the effective electron mass is smaller for the second subband in these samples. We have observed an inverse proportionality as reported by Zheng *et al.* for the mobility of electrons in the less populated second subband in Bi-containing sample annealed at 350 °C (TNBi04B). In contrast, the more populated first subband has higher electron mobility in Bi-free sample (TNR00).

The 2D electron mobility at the lowest temperature (2K) in the as-grown Bi-containing sample is ~5900 cm^2/Vs, which is closer to the electron mobility in GaAs [53] and higher than that of Bi-free sample, which can be due to the surfactant effect of Bi atoms during growth as well as lower electron density, smaller effective mass and one subband contribution to the electronic transport in Bi-containing sample. In the recent studies[54–56] as well as in our previous studies [12,13], it has been shown that the Bi atom indirectly affects electron transport parameters *via* changing the quantum confinement due to the redshift of the bandgap and Bi-related scattering events, interface roughness scattering. Since modulation doping drastically reduces the effect of ionized impurity scattering, the electron mobility in as-grown Bi-containing (TNBi04) is observed to be much higher than the reported values for Bi-containing bulk/epilayer doped with a similar density of dopants [5,6].

As seen in Figure 6, the electron mobility deteriorate after thermal annealing. The electron effective mass, the number of the occupied subbands, and electron densities are affected by the annealing process; therefore, the observed change in the electron mobility cannot be straightforwardly explained.

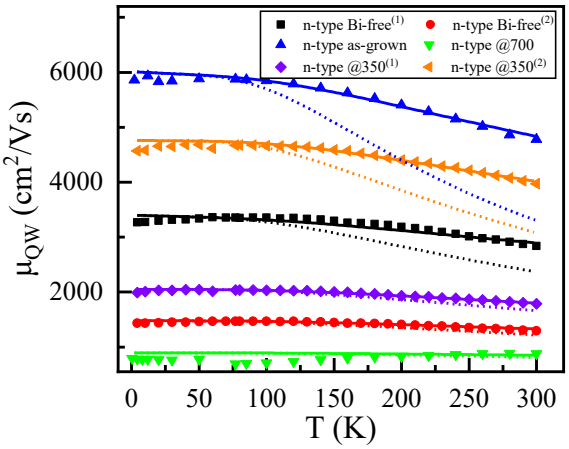

Figure 6. Temperature-dependent experimental and calculated electron mobility for all samples. Solid and dotted-lines are ascribed for calculated results with and without a multiplying factor, respectively The different symbols represent different samples. The first and second subband results for Bi-free (TNR00) and Bi-containing sample annealed at 350 °C (TNBi04B) are labeled in brackets.

The fitting parameters are given in Figure 7. The lateral height of the interface roughness increases with thermal annealing, which means the interface of the sample becomes worse after thermal annealing. Scanning electron microscopy patern show that the surface of the sample annealed 350 °C is not affected annealing treament. However, we observed the some dark area in line on the sample surface, which means the samples is deteriorated (not shonwn here). At first sight, the electron mobility of Bi-containing sample annealed at 350 °C (TNBi04B) is lower than that of the as-grown Bi-containing sample (TNBi04). However, considering the effect of carrier concentration on Hall mobility given in Table II, and eliminating the carrier concentration effect, the mobility of Bi-containing sample annealed at 350 °C (TNi04B) is higher than that of the as-grown Bi-containing (TNBi04), which agrees with the transport properties given in Ref. [12,16]. The Fermi-wave vector factor is almost constant, resulting from a similar carrier density range for all samples.

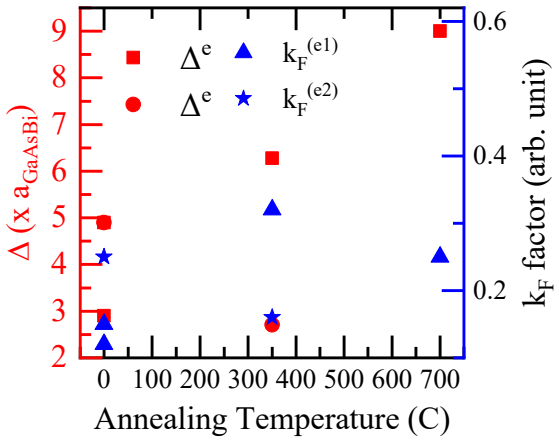

Figure 7. Used fitting parameters for all samples. The different symbols represent different samples. k_F is the Fermi-wave vector and calculated from carrier density. Δ is the height of roughness and is defined as a function of lattice constant.

Conclusions

We investigated the temperature-dependent transport properties of the modulation doped n- and p-type GaAsBi quantum structures. It is shown that electron transport occurs in multiple channels. The hole mobility at room temperature is determined as 60-95 cm^2/Vs, close to the reported value for Bi-containing alloys value, even if we could not measure at low temperature (<240K). These results also show the strong effect of Bi on the valence band of the GaAsBi alloys. Electron mobility in the as-grown Bi-containing sample is determined as 5900 cm^2/Vs. It is slightly lower than the well-known value for GaAs/AlGaAs, even this demonstrates the validity of the valence band anti-crossing model with virtual crystal contribution, the reported electron mobility value is the highest in the literature. Thermal annealing at 350 °C for 180s improves electron mobility by eliminating the effect of carrier density on electron mobility. The dominant scattering mechanism is the alloy potential mechanism, and acoustic phonon (less effective) scatterings at low temperature, and optical phonon scattering at the high-temperature region. The interface roughness scattering affects the electron mobility on the entire temperature range.

Acknowledgments

This work is supported by The Scientific and Technical Research Council of Turkey (TUBITAK) under Grant No. 115F517 and Istanbul University Scientific Research Projects Unit (Project No. FDK-2019-35447 and FDP-2020-36589).

References

[1] Arlauskas A, Svidovsky P, Bertulis K, Adomavičius R and Krotkus A 2012 GaAsBi Photoconductive Terahertz Detector Sensitivity at Long Excitation Wavelengths *Appl. Phys. Express* **5** 022601

[2] Sweeney S J and Jin S R 2013 Bismide-nitride alloys: Promising for efficient light emitting devices in the near- and mid-infrared *J. Appl. Phys.* **113** 043110

[3] Marko I P, Broderick C A, Jin S, Ludewig P, Stolz W, Volz K, Rorison J M, O'Reilly E P and Sweeney S J 2016 Optical gain in GaAsBi/GaAs quantum well diode lasers *Sci. Rep.* **6** 28863

[4] Fluegel B, Kini R N, Ptak A J, Beaton D, Alberi K and Mascarenhas A 2011 Shubnikov-de Haas measurement of electron effective mass in GaAs 1− x Bi x *Appl. Phys. Lett.* **99** 162108

[5] Kini R N, Bhusal L, Ptak A J, France R and Mascarenhas A 2009 Electron Hall mobility in GaAsBi *J. Appl. Phys.* **106** 043705

[6] Cooke D G, Hegmann F A, Young E C and Tiedje T 2006 Electron mobility in dilute GaAs bismide and nitride alloys measured by time-resolved terahertz spectroscopy *Appl. Phys. Lett.* **89** 122103

[7] Cooke D G, Young E C, Tiedje T and Hegmann F A 2007 Electron Mobility in Dilute Nitride and Bismide Alloys of GaAs *Optical Terahertz Science and Technology* (Washington, D.C., D.C.: OSA) p ME2

[8] Kini R N, Ptak A J, Fluegel B, France R, Reedy R C and Mascarenhas A 2011 Effect of Bi alloying on the hole transport in the dilute bismide alloy GaAs1-xBix *Phys. Rev. B* **83** 075307

[9] Pettinari G, Patanè A, Polimeni A, Capizzi M, Lu X and Tiedje T 2012 Bi-induced p -type conductivity in nominally undoped Ga(AsBi) *Appl. Phys. Lett.* **100** 092109

[10] Kado K, Fuyuki T, Yamada K, Oe K and Yoshimoto M 2012 High Hole Mobility in GaAs1-xBix Alloys *Jpn. J. Appl. Phys.* **51** 040204

[11] Ludewig P, Knaub N, Hossain N, Reinhard S, Nattermann L, Marko I P, Jin S R, Hild K, Chatterjee S, Stolz W, Sweeney S J and Volz K 2013 Electrical injection Ga(AsBi)/(AlGa)As single quantum well laser *Appl. Phys. Lett.* **102** 242115

[12] Donmez O, Aydın M, Ardalı Ş, Yıldırım S, Tıraş E, Nutku F, Çetinkaya Ç, Çokduygulular E,

Puustinen J, Hilska J, Guina M and Erol A 2020 Electronic transport in n-type modulation-doped AlGaAs/GaAsBi quantum well structures: influence of Bi and thermal annealing on electron effective mass and electron mobility *Semicond. Sci. Technol.* **35** 025009

[13] Donmez O, Aydın M, Ardalı Ş, Yıldırım S, Tıraş E, Erol A, Puustinen J, Hilska J and Guina M 2020 Power loss mechanisms in n-type modulation-doped AlGaAs/GaAsBi quantum well heterostructures *Semicond. Sci. Technol.* **35** 095038

[14] Ihn T 2009 *Semiconductor Nanostructures* (Oxford University Press)

[15] Kane M J, Apsley N, Anderson D A, Taylor L L and Kerr T 1985 Parallel conduction in GaAs/Al x Ga 1-x As modulation doped heterojunctions *J. Phys. C Solid State Phys.* **18** 5629–36

[16] Donmez O, Sarcan F, Lisesivdin S B, Vaughan M P, Erol A, Gunes M, Arikan M C, Puustinen J and Guina M 2014 Analytic modeling of temperature dependence of 2D carrier mobility in as-grown and annealed GaInNAs/GaAs quantum well structures *Semicond. Sci. Technol.* **29** 125009

[17] Lisesivdin S B, Yildiz A, Balkan N, Kasap M, Ozcelik S and Ozbay E 2010 Scattering analysis of two-dimensional electrons in AlGaN/GaN with bulk related parameters extracted by simple parallel conduction extraction method *J. Appl. Phys.* **108** 013712

[18] Tobin S P, Pultz G N, Krueger E E, Kestigian M, Wong K K and Norton P W 1993 Hall effect characterization of LPE HgCdTe P/n heterojunctions *J. Electron. Mater.* **22** 907–14

[19] Beck W A and Anderson J R 1987 Determination of electrical transport properties using a novel magnetic field-dependent Hall technique *J. Appl. Phys.* **62** 541–54

[20] Conwell E and Weisskopf V F 1950 Theory of Impurity Scattering in Semiconductors *Phys. Rev.* **77** 388–90

[21] Herring C and Vogt E 1956 Transport and Deformation-Potential Theory for Many-Valley Semiconductors with Anisotropic Scattering *Phys. Rev.* **101** 944–61

[22] Brooks H 1955 Theory of the Electrical Properties of Germanium and Silicon *Advances in Electronics and Electron Physics* vol 13, ed L Marton (New York: Academic Press) pp 85–182

[23] Anonymous 1951 Proceedings of the American Physical Society *Phys. Rev.* **83** 868–82

[24] Ridley B K 1977 Reconciliation of the Conwell-Weisskopf and Brooks-Herring formulae for charged-impurity scattering in semiconductors: Third-body interference *J. Phys. C Solid State Phys.* **10** 1589–93

[25] Szmyd D M, Hanna M C and Majerfeld A 1990 Heavily doped GaAs:Se. II. Electron mobility *J. Appl. Phys.* **68** 2376–81

[26] Gökden S 2003 Mobility of two-dimensional electrons in an AlGaN/GaN modulation-doped heterostructure *Phys. status solidi* **200** 369–77

[27] Ridley B K 1982 The electron-phonon interaction in quasi-two-dimensional semiconductor quantum-well structures *J. Phys. C Solid State Phys.* **15** 5899–917

[28] Ridley FRS B K 2013 Lattice scattering *Quantum Processes in Semiconductors* (Oxford University Press) pp 69–115

[29] Kearney M J and Horrell A I 1998 The effect of alloy scattering on the mobility of holes in a quantum well *Semicond. Sci. Technol.* **13** 174–80

[30] Sun Y, Balkan N, Aslan M, Lisesivdin S B, Carrere H, Arikan M C and Marie X 2009 Electronic transport in n- and p-type modulation doped Ga x In 1− x N y As 1− y / GaAs quantum wells *J. Phys. Condens. Matter* **21** 174210

[31] Vurgaftman I, Meyer J R and Ram-Mohan L R 2001 Band parameters for III–V compound semiconductors and their alloys *J. Appl. Phys.* **89** 5815–75

[32] Ben Sedrine N, Moussa I, Fitouri H, Rebey A, El Jani B and Chtourou R 2009 Spectroscopic ellipsometry study of GaAs1−xBix material grown on GaAs substrate by atmospheric pressure metal-organic vapor-phase epitaxy *Appl. Phys. Lett.* **95** 011910

[33] Ulutas K, Yakut S, Bozoglu D, Deger D, Arslan M and Erol A 2019 Influence of Bi on dielectric properties of GaAs 1−x Bi x alloys *Mater. Sci.* **37** 244–8

[34] Wang S Q and Ye H Q 2003 First-principles study on elastic properties and phase stability of III–V compounds *Phys. status solidi* **240** 45–54

[35] Tumėnas S, Karpus V, Bertulis K and Arwin H 2012 Dielectric function and refractive index of GaBix As1-x (x = 0.035, 0.052, 0.075) *Phys. status solidi* **9** 1633–5

[36] Adachi S 1985 GaAs, AlAs, and Al x Ga 1− x As: Material parameters for use in research and device applications *J. Appl. Phys.* **58** R1–29

[37] Mooney P M, Watkins K P, Jiang Z, Basile A F, Lewis R B, Bahrami-Yekta V, Masnadi-Shirazi M, Beaton D A and Tiedje T 2013 Deep level defects in n-type GaAsBi and GaAs grown at low temperatures *J. Appl. Phys.* **113** 133708

[38] Mooney P M, Tarun M, Beaton D A, Mascarenhas A and Alberi K 2016 Deep level defects in dilute GaAsBi alloys grown under intense UV illumination *Semicond. Sci. Technol.* **31** 085014

[39] Luo G, Yang S, Jenness G R, Song Z, Kuech T F and Morgan D 2017 Understanding and reducing deleterious defects in the metastable alloy GaAsBi *NPG Asia Mater.* **9** e345–e345

[40] Jiang Z, Beaton D A, Lewis R B, Basile A F, Tiedje T and Mooney P M 2011 Deep level defects in GaAs 1− x Bi x /GaAs heterostructures *Semicond. Sci. Technol.* **26** 055020

[41] Gelczuk Ł, Kopaczek J, Rockett T B O, Richards R D and Kudrawiec R 2017 Deep-level defects in n-type GaAsBi alloys grown by molecular beam epitaxy at low temperature and their influence on optical properties *Sci. Rep.* **7** 12824

[42] Fuyuki T, Kashiyama S, Tominaga Y, Oe K and Yoshimoto M 2011 Deep-Hole Traps in p-Type GaAs1-xBix Grown by Molecular Beam Epitaxy *Jpn. J. Appl. Phys.* **50** 080203

[43] Lu X, Beaton D A, Lewis R B, Tiedje T and Whitwick M B 2008 Effect of molecular beam epitaxy growth conditions on the Bi content of GaAs1−xBix *Appl. Phys. Lett.* **92** 192110

[44] Millunchick J M and Tait C R 2019 Surface Mediated Growth of Dilute Bismides pp 201–14

[45] Pillai M R, Kim S-S, Ho S T and Barnett S A 2000 Growth of In[sub x]Ga[sub 1−x]As/GaAs heterostructures using Bi as a surfactant *J. Vac. Sci. Technol. B Microelectron. Nanom. Struct.* **18** 1232

[46] Ihn T 2009 Magnetotransport in two-dimensional systems *Semiconductor Nanostructures* (Oxford University Press) pp 287–334

[47] Cetinkaya C, Cokduygulular E, Nutku F, Donmez O, Puustinen J, Hilska J, Erol A and Guina M 2018 Optical properties of n- and p-type modulation doped GaAsBi/AlGaAs quantum well structures *J. Alloys Compd.* **739** 987–96

[48] Liu W C 1990 Investigation of electrical and photoluminescent properties of MBE-grown Al x Ga1?x As layers *J. Mater. Sci.* **25** 1765–72

[49] Donmez O, Sarcan F and Erol A 2021 Determination of the acoustic phonon-hot carriers interaction in n- and p-type modulation-doped GaInNAs/GaAs quantum wells *Phys. B* **612** 412946

[50] van Houten H, Williamson J G, Broekaart M E I, Foxon C T and Harris J J 1988 Magnetoresistance in a GaAs-AlxGa1-xAs heterostructure with double subband *Phys. Rev. B* **37** 2756–8

[51] Ahn I-H, Song G H and Jho Y-D 2010 Separating the Contribution of Mobility among Different Quantum Well Subbands *Jpn. J. Appl. Phys.* **49** 014102

[52] Zheng Z W, Shen B, Jiang C P, Gui Y S, Someya T, Zhang R, Shi Y, Zheng Y D, Guo S L, Chu J H and Arakawa Y 2003 Multisubband transport of the two-dimensional electron gas in AlxGa1−xN/GaN heterostructures *J. Appl. Phys.* **93** 1651–5

[53] Blakemore J S 1982 Semiconducting and other major properties of gallium arsenide *J. Appl. Phys.* **53** R123–81

[54] Donmez O, Kara K, Erol A, Akalin E, Makhloufi H, Arnoult A and Fontaine C 2016 Thermal annealing effects on optical and structural properties of GaBiAs epilayers: Origin of the thermal annealing-induced redshift in GaBiAs *J. Alloys Compd.* **686** 976–81

[55] Grant P C, Fan D, Mosleh A, Yu S-Q, Dorogan V G, Hawkridge M E, Mazur Y I, Benamara M, Salamo G J and Johnson S R 2014 Rapid thermal annealing effect on GaAsBi/GaAs single quantum wells grown by molecular beam epitaxy *J. Vac. Sci. Technol. B* **32** 02C119

[56] Mohmad A R, Bastiman F, Hunter C J, Richards R, Sweeney S J, Ng J S and David J P R 2012 Effects of rapid thermal annealing on GaAs 1-x Bi x alloys *Appl. Phys. Lett.* **101** 012106